Vibrationally induced flip motion of a hydroxyl dimer on Cu(110)

Yasuhiro Ootsuka

Division of Nano and New Functional Material Science, Graduate School of Science and Engineering,
University of Toyama, Toyama, 930-8555 Japan

Thomas Frederiksen

Donostia International Physics Center (DIPC), ES-20018 San Sebastián, Spain

Hiromu Ueba

Division of Nano and New Functional Material Science, Graduate School of Science and Engineering,
University of Toyama, Toyama, 930-8555 Japan

Magnus Paulsson[*]

School of Computer Science, Physics and Mathematics, Linnaeus University, SE-391 82 Kalmar, Sweden

Recent low-temperature scanning-tunneling microscopy experiments [T. Kumagai *et al*., Phys. Rev. B **79**, 035423 (2009)] observed the vibrationally induced flip motion of a hydroxyl dimer $(OD)_2$ on Cu(110). We propose a model to describe two-level fluctuations and current-voltage characteristics of nanoscale systems that undergo vibrationally induced switching. The parameters of the model are based on comprehensive density functional calculations of the system's vibrational properties. For the dimer $(OD)_2$, the calculated population of the high- and low-conductance states, the I-V, dI/dV, and d^2I/dV^2 curves are in good agreement with the experimental results and underline the different roles played by the free and shared OD stretch modes of the dimer.

Electron transport through single-molecule junctions has been receiving enthusiastic interest for a development of novel molecular devices. Nonlinear I-V characteristics associated with the vibrationally mediated configurational change with different conductances have been observed in a series of systems such as pyrrolidine on a Cu(001),[1] H_2 on Cu,[2] CO bridging a Pt contact,[3] and H_2 in Au contacts.[4] In these systems, dI/dV spectra show anomalous spikes—in contrast to steps usually observed in the inelastic electron tunneling spectroscopy (IETS)[5]—at the bias voltage related to the vibrational mode energies.

Recently Kumagai *et al*.[6] studied the dynamics of a single hydroxyl (OH, OD) molecule and the dimer $(OD)_2$ on Cu(110) using a scanning tunneling microscope (STM). The STM images observed for the monomer suggested a possible quantum tunneling of a hydroxyl between two equivalent adsorption configurations on Cu(110), as supported by the density functional theory (DFT) calculations of the transition path and rate of the flipping of OH on Cu(110).[7] This spontaneous flip motion of hydrogen atoms in the monomer is quenched for the dimer at low temperatures, but can be induced by excitation of the OH/OD stretch mode by tunneling electrons. Time-averaged measurements of the current show a nonlinear current (I) increase at the bias voltage (V) inducing the transition between the high- and low-conductance states. The appearance of the peak in dI/dV and the peak and dip in d^2I/dV^2 from transitions between states with distinct conductances have also been reported previously.[2–4]

In this paper, a combined use of the DFT-based SIESTA,[8] TRANSIESTA,[9] and INELASTICA[10,11] packages permits us to gain insight into the elementary processes that induce the flip motion of the asymmetric dimer. The extensive DFT calculations provide the ground-state geometry, vibrational modes, electron-vibration couplings, emission rate of vibrations from tunneling electrons, vibrational damping due to electron-hole pair excitation, and the high and low conductance. These calculated properties allow us to model the population of the high- and low-conductance states as a function of the bias voltage and the nonlinear I-V characteristics for $(OD)_2$ on a Cu(110) surface. The experimental results (relative occupation of the high- and low-conductance state, I-V curve, and dI/dV) are nicely reproduced, and the different roles played by the free and shared OD stretch modes in the vibrationally mediated configurational flip motion are clarified.

The telegraph switching between high- and low-conductance states of $(OD)_2$ is shown schematically in Fig. 1. In low-temperature STM, no spontaneous switching is observed at low bias since the barrier for the reaction is substantial.[6] Keeping the STM tip stationary and increasing the bias over approximately 200 meV, the switching between the two degenerate low-energy configurations is triggered by phonon emission. However, the reaction rate remains rather small until the bias exceeds the ν(OD) stretch vibrations ($\approx$300–330 meV). We denote the two configurations as the high (H) and low (L) conductance states where the tip-dimer distance is smaller for the H configuration.

To investigate the flip motion of the dimer $(OD)_2$, we performed calculations on a six-atom thick Cu 4×3 slab using periodic boundary conditions. The tip was modeled as one protruding Cu atom on the reverse side of the slab. All calculations were performed with the PBE GGA functional, DZP (SZP) basis set for dimer (bulk Cu), 3×4 k-point
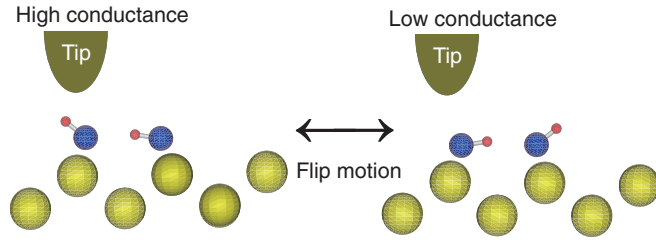
FIG. 1. (Color online) Schematic view of the high- and low-conductance states of the dimer (OD)$_2$ on Cu(110). Yellow, blue, and red circles are Cu, O, and D atoms, respectively. See text for details on the relaxed geometry.

sampling, and a 300 Ry mesh cutoff. The elastic transport properties were calculated using the DFT + NEGF method[9] where six additional layers of Cu were used to connect the central region to semi-infinite metallic leads. Figure 1 shows the schematic side view of the dimer in the H and L conductance states. The calculated low-bias conductance ratio $G_H/G_L = 2.0$ closely matches the experimental ratio. However, the calculated absolute conductances are much larger than in the experiment since numerical considerations demand the calculations to be performed at a small tip-dimer distance. The relaxed hydrogen-bonded OD-O distance is 2.90 Å, while the OD bond length and tilt angle to the surface normal are 1.00 (0.98) Å and 81° (51°), respectively. The two hydroxyl groups, bonded near adjacent bridge sites along (001), are oriented according to the optimal configuration for hydrogen bonding. The D atom pointing toward the adjacent OD molecule forms the OD-O bond (with a characteristic shared OD stretch mode) in contrast to the D atom pointing away from the adjacent OD molecule (with a free OD stretch mode). These nonequivalent configurations of each OD molecule lift the degeneracies of the vibrational energies for the two OD molecules.

The vibrational modes and frequencies of the molecular adsorbates and the corresponding electron-phonon couplings are calculated from a finite-difference scheme.[10,11] These calculations were repeated with the tip scanned over the surface as indicated by the black dots in Fig. 2. Table I lists the calculated vibrational modes for the H and L configurations. Here, ν(OD) labels the free OD stretch mode, ν(OD-O) is the shared OD stretch mode involving the D atom between two oxygen atoms, and rot$_{xy(z)}$ are the rotation modes in the surface plane (surface normal). Values for the low-energy modes mainly involving motion of the oxygen atoms have been omitted from the table.

In addition to the vibrational energies ($\hbar\omega$), the electron-hole pair damping rate γ_{eh} and vibration generation rate γ_{em} were calculated for each tip position within the lowest order expansion (LOE) scheme.[10,11] In the low-temperature limit, the emission rate is given by

$$\gamma_{em}(V) = \lambda_{em}\left(|eV| - \hbar\omega\right)\theta\left(|eV| - \hbar\omega\right), \quad (1)$$

where V is the applied bias, θ is the step function, and $\lambda_{em} = \frac{1}{\pi\hbar}\text{Tr}[\mathbf{M}\mathbf{A}_1\mathbf{M}\mathbf{A}_2] = \frac{4\pi}{\hbar}\sum_{\alpha\beta}|\langle\psi_\beta^2|\mathbf{M}|\psi_\alpha^1\rangle|^2$ is the emission rate constant written in terms of electron-phonon coupling matrix $\mathbf{M}$ and partial spectral density $\mathbf{A}_{1/2}$ at the Fermi energy, cf. Ref. 10. The spectral density can further be rewritten in
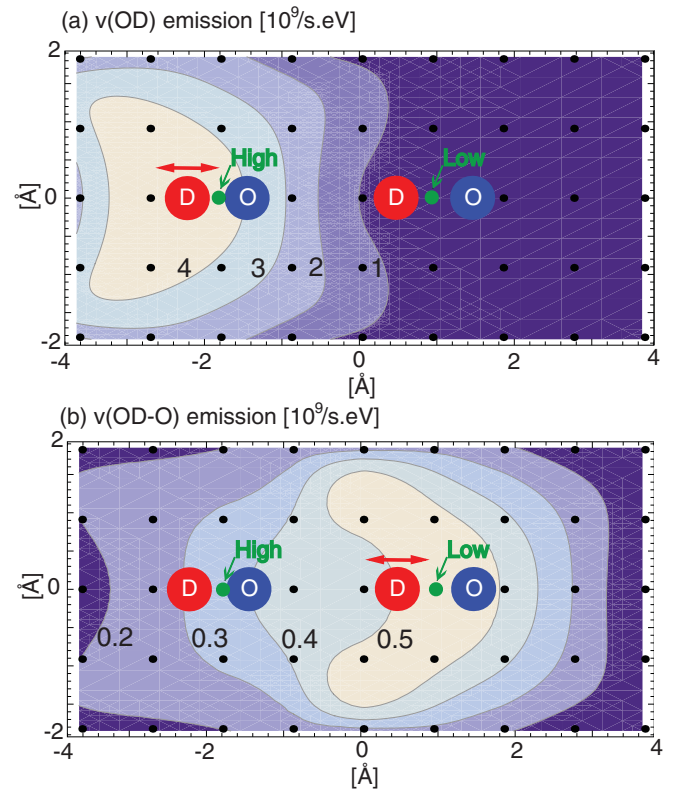

FIG. 2. (Color online) (a) Emission rate constant $\lambda_{em,\nu(OD)}$ of the free ν(OD) stretch and (b) $\lambda_{em,\nu(OD-O)}$ of the shared ν(OD-O) stretch mode. The blue and red circles are O and D atoms, respectively. The black doted grids are the tip position fixed at 5.6 Å above the oxygen atom and the red arrows indicate the vibrational motion. The values of the contour lines are indicated in the figures [$10^9/(s~eV)$] and the exact values with the tip positioned at the large green dots are listed in Table I.

terms of a sum over scattering states $|\psi_\alpha^{1/2}\rangle$ at the Fermi-energy incident from substrate/tip (1/2) showing the equivalence of the LOE scheme with the Fermi-golden rule, assuming a constant density of states around the Fermi-energy.[10] Furthermore, for weak coupling between tip and adsorbate, the emission rate constants scale with the tip-adsorbate coupling (τ) squared ($\lambda \propto \tau^2$). Since the current scales in the same way, the emission rate at a given voltage is proportional to the current. On the contrary, the electron-hole pair damping rate γ_{eh} is insensitive to the position of the STM tip since the damping is dominated by the metal surface. The emission rate maps for the two ν(OD) and ν(OD-O) modes are shown in Fig. 2, where the emission rates were calculated by scanning the tip over the surface at a constant height of 5.6 Å above the oxygen atoms, i.e., the DFT calculations of electron-phonon coupling, transmission, emission rates, and damping were repeated for geometries with the tip displaced relative to the OD dimer. We note that the emission rate for the free OD stretch is more localized around the high conductance site than the shared OD-O stretch mode, which is also evident from Table I. The green points in Fig. 2 correspond to the H and L configurations listed in Table I.

To describe vibrationally induced switching in nanoscale systems, we propose a simple model that expresses the current in terms of the occupation $n_{H(L)}$ and conductance $\sigma_{H(L)}$ of the

TABLE I. Vibrational mode frequencies, emission rate constants and their electron-hole pair damping rates at H and L conductance state.

Mode	$\hbar\omega$ (meV)	λ_{em} [10^9/(s eV)]	γ_{eh} (10^9/s)
ν(OD) L	327.2	0.17	47.3
ν(OD) H	326.6	4.42	52.3
ν(OD-O) L	301.2	0.49	248.0
ν(OD-O) H	301.8	0.35	249.6
rot$_z$(OD-O) L	76.8	1.19	250.7
rot$_z$(OD-O) H	76.5	0.67	268.0
rot$_{xy}$(OD-O) L	77.0	0.24	103.7
rot$_{xy}$(OD-O) H	76.9	0.10	76.0
rot$_{xy}$(OD) L	51.8	0.01	59.4
rot$_{xy}$(OD) H	52.6	0.71	60.7
rot$_z$(OD) L	49.9	0.27	97.0
rot$_z$(OD) H	49.8	0.79	86.6

H and L conductance states,

$$I = \sigma_H n_H(V)V + \sigma_L n_L(V)V, \qquad (2)$$

where $n_{H(L)}$ is determined as a stationary solution of the rate equations,

$$dn_H/dt = \Gamma^{L\to H}(V)n_L - \Gamma^{H\to L}(V)n_H, \qquad (3)$$

$$dn_L/dt = \Gamma^{H\to L}(V)n_H - \Gamma^{L\to H}(V)n_L, \qquad (4)$$

with the condition $n_H + n_L = 1$. This gives

$$n_L(V) = \frac{\Gamma^{H\to L}}{\Gamma^{H\to L} + \Gamma^{L\to H}}, \quad n_H(V) = \frac{\Gamma^{L\to H}}{\Gamma^{H\to L} + \Gamma^{L\to H}}, \qquad (5)$$

where $\Gamma^{H\to L}$ is the transition rate from H to L. The experiments show that the reaction rate at a constant voltage is proportional to the current, i.e., the reaction rate is proportional to the emission rate of the vibrations. The simplest way to model the transition rates is therefore to assume a linear dependence on the vibrational occupation γ_{em}/γ_{eh} or equivalently the vibrational generation rates γ_{em},[13] i.e.,

$$\Gamma^{H\to L(L\to H)}(V) = \Gamma_0^{H(L)} + \sum_i C_i \Gamma_{em,i}^{H(L)}(V), \qquad (6)$$

where a constant rate $\Gamma_0^{H(L)}$ is introduced to model the collective effect of many low-energy vibration modes and where $\Gamma_{em,i}^{H(L)}$ represents the broadened vibrational generation rate[12] of a mode with a distinct frequency Ω_i given by

$$\Gamma_{em,i}^{H(L)} = \int_0^\infty W(\omega - \Omega_i^{H(L)}, \sigma_{ph}^i)\gamma_{em,i}(eV,\omega)d\omega. \qquad (7)$$

In the above equation, we use a Gaussian distribution function $W(\omega,\sigma_{ph}) \propto e^{-\omega^2/(2\sigma_{ph}^2)}$ characterized by a standard deviation σ_{ph}. The prefactors C_i describe the likelihood of the generated vibrational excitation to induce the flip motion, i.e., the probability of transferring the motion from the vibration to the reaction coordinate.[13]

We obtain a good fit to the experimental OD dimer data from Ref. 6 considering only three different vibrational modes, see Fig. 3. The fitting parameters used ($C_i, \hbar\Omega_i^{H/L}, \sigma_{ph}^i$) are
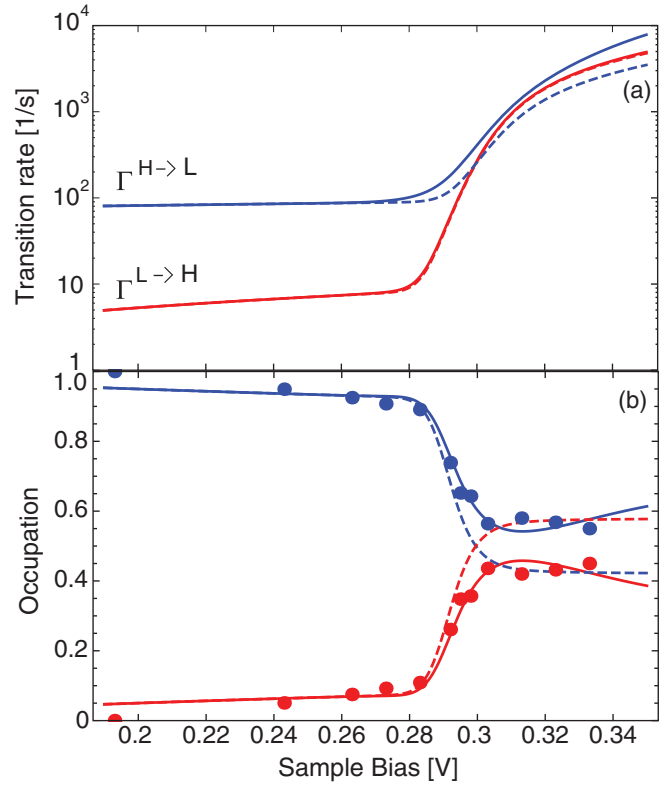

FIG. 3. (Color online) (a) Calculated transition rates $\Gamma^{H\to L(L\to H)}(V)$ and (b) occupations H (red) and L (blue) configurations of a dimer (OD)$_2$ on Cu(110). See text for the parameters used to fit the experimental occupations from Ref. 6 (blue/red dots). The dashed curves are calculated without the contribution of the free OD stretch mode.

(0.2×10^{-4}, 327.2/326.6 meV, 20 meV) for ν(OD), (1.0×10^{-4}, 301.2/301.8 meV, 8 meV) for ν(OD-O), (1.2×10^{-7}, 76.8/76.5 meV, 19 meV) for rot$_z$(OD-O), and $\Gamma_0^{H/L} = 0.7 \times 10^2/1 \times 10^{-4}$ s^{-1}. We first note that we need to use large values for the broadening $\sigma_{ph}^i \sim 10$–20 meV to fit the experimental data. We believe this to be caused by the statistical nature of the experimental data collection and do not reflect thermal or phonon DOS broadening.[12] The fitting constants C_i and $\Gamma_0^{H/L}$ are only determined up to a multiplicative factor since the occupations are determined by the ratios in Eq. (5). We choose the prefactor of the shared ν(OD-O) mode as the reference and set it to 10^{-4} based on an order of magnitude estimate from the experimental flip frequency.[6] The values for $\Gamma_0^{H/L}$ only determine the low-bias occupation where $\Gamma_0^H \gg \Gamma_0^L$ because the system is experimentally only observed in the L configuration. The reason for this preference of L at low bias might be due to the larger current and thus larger vibrational generation rate of low-energy phonons in the H configuration. However, in the intermediate bias range $200 \sim 300$ meV we see a slight change in the occupation as shown in Fig. 3(b). Although we cannot unambiguously assign a vibrational mode to this change in occupation from the available experimental data, we have chosen to model this by the rot$_z$(OD-O) mode. In contrast, there is much less latitude in the fitting parameters for the ν(OD) and ν(OD-O) modes. We note that the change in occupation at 300 meV does not fit with

the free ν(OD) vibrational energy ($\approx$330 meV) and clearly indicates that the shared ν(OD-O) mode is the main culprit in inducing the flip motion. This assignment is supported by the fact that the occupation quickly approaches 50/50, which implies that the emission rate constants λ_{em} of the high- and low-conductance states are of similar magnitude. This is clearly not the case for the free ν(OD) but true for the ν(OD-O) mode, see Table I and Fig. 2. To underline the effects of the shared ν(OD-O) and free ν(OD) stretch modes, Fig. 3 shows the full modeling (solid line) and without the free ν(OD) vibration (dashed line). Without the ν(OD) mode, the occupation rapidly approaches the ratio of the shared ν(OD-O) emission rate constants $n_L/n_H \xrightarrow[[eV \gg \hbar\omega]]{} \lambda_{em}^H/\lambda_{em}^L \approx 0.71$. Note that the approximately equal occupation of the H/L states is a coincidence and that the ratio of the occupations at high bias is simply given by the ratio of emission rate constants and the fitting constants C_i. In contrast to the shared ν(OD-O) mode, which increases the H state occupation, the main effect of the free ν(OD) mode is a slight increase of the $H \rightarrow L$ transition rate, see Fig. 3(a), and thereby slightly decreases the occupation of the H state.

Using the calculated conductances (σ_H = 145.62 nA/V, σ_L = 78.34 nA/V) scaled by the constant factor 2.56×10^{-2} to account for the small tip-sample distance used in the calculation and the bias-dependent population $[n_H(V), n_L(V)]$ shown in Fig. 3(b), the I-V characteristics were calculated from Eq. (2). As shown in Fig. 4, the calculated time-averaged I-V curve [Fig. 4(a)] and d^2I/dV^2 [Fig. 4(b)] show remarkable agreement with the experimental results. We note that the lineshape of the d^2I/dV^2 signal is clearly different from inelastic electron tunneling spectra, which normally only show a peak or dip.[14] In addition, the size of the signal from the vibration is much larger than what one normally associates with inelastic electron tunneling spectroscopy (IETS) spectra.

In summary, we have shown that the flip motion between high- and low-conductance configuration of the OD dimer on Cu(110) is mainly induced by the excitation of the hydrogen-bonded shared OD stretch mode. Because of the unique asymmetric inclined orientation of each hydroxyl, the shared and free OD stretch modes have different vibrational frequencies and consequently affect the flip motion at different applied bias voltages. The relative occupations (n_H and n_L) of the high- and low-conductance states as a function of the bias voltage were nicely reproduced by solving a simple rate equation for n_H and n_L in terms of the transition rate
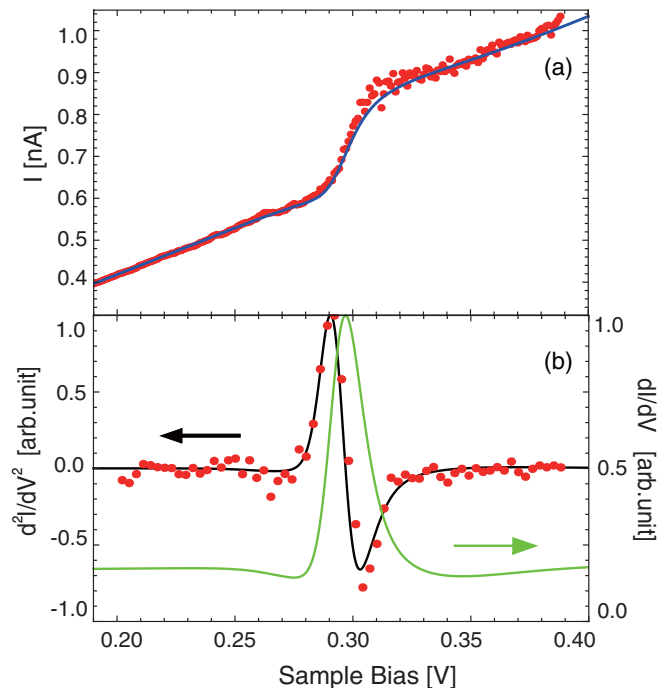

FIG. 4. (Color online) (a) I-V curve (blue line: calculation, red dots: experiment) and (b) dI/dV (green line: calculation) and d^2I/dV^2 (black line: calculation, red dots: experiment). The experimental data originate from Ref. 6.

between the H and L configurations. The calculated high and low conductances (σ_H, σ_L) and their occupations [$n_H(V)$, $n_L(V)$] enabled us to obtain the nonlinear I-V curve, dI/dV, and d^2I/dV^2 in excellent agreement with the experimental results. The presented theoretical analysis based on extensive DFT calculations (stable configurations, vibrational modes including their generation rates by tunneling electrons, and damping rates) is not limited to the specific case of hydroxyl dimers on Cu(110), but can also be applied to other systems that exhibit nonlinear I-V characteristics arising from the vibrationally mediated switching between high- and low-conductance states.

*magnus.paulsson@lnu.se

[1] J. Gaudioso, L. J. Lauhon, and W. Ho, Phys. Rev. Lett. **85**, 1918 (2000).

[2] J. A. Gupta, C. P. Lutz, A. J. Heinrich, and D. M. Eigler, Phys. Rev. B **71**, 115416 (2005).

[3] W. H. A. Thijssen, D. Djukic, A. F. Otte, R. H. Bremmer, and J. M. van Ruitenbeek, Phys. Rev. Lett. **97**, 226806 (2006).

[4] A. Halbritter, P. Makk, Sz. Csonka, and G. Mihály, Phys. Rev. B **77**, 075402 (2008); M. L. Trouwborst, E. H. Huisman, S. J. van der Molen, and B. J. van Wees, ibid. **80**, 081407(R) (2009); M. Kiguchi,

T. Nakazumi, K. Hashimoto, and K. Murakoshi, ibid. **81**, 045420 (2010).

[5] B. C. Stipe, M. A. Rezaei, and W. Ho, Science **280**, 1732 (1998).

[6] T. Kumagai, M. Kaizu, H. Okuyama, S. Hatta, T. Aruga, I. Hamada, and Y. Morikawa, Phys. Rev. B **79**, 035423 (2009).

[7] E. R. M. Davidson, A. Alavi, and A. Michaelides, Phys. Rev. B **81**, 153410 (2010).

[8] P. Ordejón, E. Artacho, and J. M. Soler, Phys. Rev. B **53**, R10441 (1996); J. M. Soler et al., J. Phys. Condens. Matter **14**, 2745 (2002).

[9]M. Brandbyge, J. L. Mozos, P. Ordejón, J. Taylor, and K. Stokbro, Phys. Rev. B **65**, 165401 (2002).

[10]T. Frederiksen, M. Paulsson, M. Brandbyge, and A.-P. Jauho, Phys. Rev. B **75**, 205413 (2007).

[11]The Inelastica software is freely available at [http://sourceforge.net/projects/inelastica/].

[12]K. Motobayashi, Y. Kim, H. Ueba, and M. Kawai, Phys. Rev. Lett. **105**, 076101 (2010).

[13]H. Ueba, S. G. Tikhodeev, and B. N. J. Persson, in *Current-Driven Phenomena in Nanoelectronics*, edited by T. Seideman (Pan Stanford Publishing, Singapore, 2010).

[14]M. Paulsson, T. Frederiksen, and M. Brandbyge, Phys. Rev. B **72**, 201101 (2005).